A multi-method approach for characterizing landslides in an intramontane basin of Andes (Loja, Ecuador)

John Soto(1,2), Jorge P. Galve(2), José Antonio Palenzuela(3), José Miguel Azañón(2), José Tamay(1), Clemente Irigaray(3)

(1) Departamento de Geología y Minas e Ingeniería Civil. Universidad Técnica Particular de Loja. San Cayetano Alto s/n, Loja Ap.1101608, Ecuador.
(2) Departamento de Geodinámica, Universidad de Granada, Campus Fuentenueva s/n, Granada 18071, Spain.
(3) Departamento de Ingeniería Civil, ETSICCP, Universidad de Granada. Campus Fuentenueva s/n, Granada 18071, Spain.

Abstract

In the last decades, growing population in the Andean cities has generated the urban expansion over landslide-prone areas. Fatal landslides affecting urban settlements are specially frequent in the cities located in the Neogene intramontane basins of Andes. These basins show similar geographical and geological features that frequently generate ground instability situations. We studied the characteristics of the mass movements observed in these basins by carrying out a detailed analysis of four landslides occurred in the Loja Basin (Ecuador). This multi-method study integrated DGPS, ERT, geotechnical methods, a mineralogical study and time-series analyses of precipitation. Our study characterize the slope movements as active slow-moving complex earth-slides earth-flows. According to DGPS measurements, these landslides move at velocities up to several meters per year. ERT profiles show that most of the landslides are mainly surficial. Time-series analyses of precipitation reveal that not exceptionally intensive rainfall events can reactivate these landslides. This characteristic and the development of these landslides in low gradient slopes was explained by the results obtained through geotechnical and mineralogical analyses. We find that smectite clay minerals detected in the mobilized geological formations combined with the tropical climate of the northern Andean region induce the observed weak slope stability conditions. The conceptual model for the studied landslides may aid in assessing landslide-prone areas in Loja and other Neogene intramontane basins of Andes, and

helping in the mitigation of the associated risk.

Keywords
Landslides, DGPS, ERT, Geotechnics, Clay minerals, Time-series analysis

1. Introduction

The urban growth in the Andean cities has increased the exposition of population to landslides. This growth demands new terrain for urban development and led to the deforestation and occupation of hillsides. First, deforestation is one of the main factors that cause shallow landsliding and intensify torrent-related phenomena. Second, the urbanization of hillsides is always linked to an implicit risk to landslides because the poor ground conditions of the slopes. These slope stability conditions are worse where the humid climate of tropical and subtropical latitudes enhance rock weathering. If we add to that the frequent earthquakes that struck the northern Andean region, the result is one of the world's region with the highest density of fatal landslides (Petley 2012).The serious consequences of this are reflected in the number of casualties and economic losses due to landslides reported in this region (Fig. 1, Table 1).

A large number of fatal landslides occur in a specific geological setting within the Andean Cordillera, the Neogene intramontane basins. These basins embrace similar geographical and geological characteristics that explain the high incidence of these phenomena. They feature humid tropical climate and exhibit fine-grained, continental sedimentary rocks deposited in fluvial and lacustrine environments, when combined, frequently generate ground instability conditions. The latter combined with the rapid urban development evolved in those areas results in a high landslide risk situation. Although landslides have high impacts at a societal and economical level, comprehensive studies of mass movements have not been carried out in these areas. Most of the published studies are focused on general descriptions of specific cases (e.g. PMA 2007), putting aside detailed geotechnical, geophysical or kinematic analyses.

This study seeks to characterize and contextualize the usual mass movements observed in an Andean Neogene intramontane basin. We have approaching this study analyzing in detail four active landslides in the city of Loja (Ecuador). We applied different techniques to provide information about the main characteristics of these landslides. Kinematics were studied by carrying out a DGPS (Differential Global Positioning System) monitoring (e.g. Tagliavini et al. 2007; Acar et al. 2008; Acar 2010; Zarate

2011; Calcaterra et al. 2012; Dogan et al. 2012). GPS-based methods are effective to measure displacements in landslides (Gili et al. 2000; Malet et al. 2002; Mora et al. 2003; Giordan et al. 2013) because allow to perform measurements up to milimeters per year (Zhou et al. 2005). Nowadays, they are neither too expensive nor too demanding techniques where a continuous monitoring is not required (e.g., Rizzo 2002; Brückl et al. 2006; Noferini et al. 2007; Coltorti et al. 2011). The geometry of the landslide mass, failure planes and areas characterized by high water content were established analyzing longitudinal and transversal ERT (Electrical Resistivity Tomography) profiles (e.g. Lapenna et al. 2003; 2005; Travelletti et al. 2009; Hibert et al. 2012; Colangelo et al. 2008; Colangelo and Perrone 2012). Causal factors were established through geotechnical and mineralogical characterization of the materials involved in the landslides (e.g. Yilmaz and Karacan 2002; Azañón et al. 2010; Garrido and Delgado 2012; Grana and Tommasi 2014). Landslide triggering or reactivation rainfall thresholds were defined applying a precipitation time-series analysis. This analysis was addressed by a simple comparison between the cumulative rainfall recorded during the wet period related to every landslide and the mean rainfall for the same period when considering the existing rainfall series (1964 - 2014) for the study area (e.g. Irigaray et al. 2000; Irigaray and Palenzuela 2013; Palenzuela et al. 2015). This is the first case in Latin America that a comprehensive landslide characterization is published in the international scientific literature. The application of ERT to landslides in this region was not previously described at the international level (cf. Perrone et al. 2014) and the integration of different techniques entails a great novelty in the Andean setting.

2. Geographical and geological setting

Loja is located in the southern Ecuadorian Andean region (Fig. 2). The city has grown in the headwaters of the Zamora River taking advantage of a wide valley situated at about 2100 m a.s.l. This valley show an unusual enlargement because was carved into the materials deposited in an intramontane sedimentary basin called Loja Basin uplifted to high elevations by tectonic forces. Currently, the sediments of this basin show a moderate deformation but the area still roughly maintains its basin morphology.

The Loja Basin is one of the Neogene intramontane basins (Azogues-Cuenca-Nabón, Loja, Malacatos-Vilcabamba and Catamayo) described in the southern Ecuador that conditioned the relief of the Andean cordillera in this region (Hungerbühler et al. 2002;

Galindo-Zaldívar et al. 2010). These basins were formed associated to the crustal thinning occurred during the Miocene accompanied by the subsidence of the areas located in the South of the actual Ecuador (Kennerley 1980; Hungerbühler et al. 2002). The Pacific transgression of these basins deposited marine sediments that were deformed during the Late Miocene in a subsequent deformational phase dominated by a general compression (Hungerbühler et al. 2002). This compressional period is characterized in the Loja Basin by the sedimentation of continental deposits formed by fluvial, deltaic and lacustrine facies and the synsedimentary folding and normal faulting observed in its occidental part (Hungerbühler et al. 2002). The last sedimentary record is composed of alluvial fan deposits unconformably deposited over the Miocene sediments during the Upper Miocene (Hungerbühler et al. 2002).

The sedimentary rocks that outcrop in the Loja Basin comprise six main formations (Hungerbühler et al. 2002). The lowermost sedimentary series described in the valley of Loja is the Trigal Formation (Middle Miocene), which consist of subhorizontal coarse-grained sandstones with interbedded siltstones and conglomerates, the latter with fine volcanic clasts. This formation ranges from 50 to 150 m in thickness from the west to the east of the basin and was interpreted as fluvial deposits. The other five stratigraphic units exposed in the valley include, in ascending order: (1) The La Banda Formation (Middle Miocene), a sequence of lacustrine deposits, 10-20 m thick, composed of thick beds of massive limestones and layers of marls, cherts and yellow fine sandstones. (2) The Belén Formation (Middle Miocene), a sandstone with inter-layered conglomerate and shale strata, up to 300 m thick; this formation was interpreted as a transition from a lagoonal to a deltaic and mixed-load fluvial environment (Hungerbühler et al. 2002). (3) The San Cayetano Formation (Middle Miocene), which is a 800 m thick sequence subdivided into three members: the Lower Sandstone Mb. composed of sandstone and channelized conglomerates beds with minor layers of shales and coal seams; the Siltstone Mb. which is characterized by laminated brown, grey and white shales partly silicified, abundant diatomite layers, and a few pyroclastic horizons; and the Upper Sandstone Mb., which is broadly similar to the Lower Sandstone Mb. showing finer grained deposits and a coarsening-upward trend; these deposits reflect an environment that starts with a freshwater lagoon system and a subsequent contribution of a mixed-load fluvial system. (4) The Quillollaco Formation (Late Miocene), a metamorphic clast-supported conglomerates and lensshaped sandstones deposited in alluvial fan

environments with up to 600 m in thickness. (5) The Zalapa Formation (Pliocene), which consist of about 10 m thick weathered tuffs that crop out only in the NW area of the Loja Basin. These Miocene to Pliocene sedimentary formations lie over Paleozoic metamorphic rocks consisting of quartzites, phyllites, slates and schists (Litherland et al. 1994).

As mentioned above, the geological structures and materials that constitute the Loja Basin have controlled the landscape of the valley of Loja. This anomalous high and wide valley has a N-S direction and show a maximum width of about 14 km (distance between ridgelines). The Oriental Range of the Andes flanks the valley to the east with peaks reaching more than 3200 m a.s.l. and show abrupt and narrow valleys. To the west, the valley is bounded by the Villonaco Range, a lower mountain chain with elevations about 2700 m a.s.l. that is part of the Continental Divide of the Americas. This range show gradual slopes and low local relief in its east flank towards the Loja Valley and steep and incised basins to the west. The mentioned ranges consist of Paleozoic metamorphic rocks uplifted by orogenic processes. The bottom of the valley, at about 2100 m a.s.l. and 7 km wide, shows a low hilly landscape dominated by a cuesta-relief. This landscape was conditioned by the slightly tilted and folded beds of the Loja Basin infill sediments. The NW of the area is covered by a colluvium, locally called “denudativo” (Fig. 2). This deposit was derived from the erosion of the metamorphic reliefs but its origin is controversial. Although Loja is in the headwaters of the Zamora and Malacatos rivers, these water courses have developed an alluvial plain, less than a kilometre wide, at the bottom of the valley. This plain is endangered by recurrent floods, which affect regularly some areas of the city during intense rainfall events.

The climate of Loja is characterized by humid subtropical conditions with average annual rainfall of 917 mm and a mean monthly temperature between 14°C and 24ºC. A high proportion of the rain falls from December to April. Thus, the period from May to November is defined as the dry season, though precipitation continues throughout the year but less frequently. Storms or high precipitation periods are usual during the humid season and they are responsible of floods and torrent-related phenomena.

In addition to the above-mentioned floods, Loja Valley is also affected by numerous landslides. They are mainly associated to the clays, siltstones and colluvial deposits of the Loja sedimentary basin and are also triggered by intense rainfall events or periods of high precipitation. The size of the most characteristic landslides of Loja have lengths ranging from 100 to 250 m and widths ranging from 60 to 150 m, but has been mapped landslides that reach 1200 m long and 250 m wide. Most of the landslides mobilized volumes between 15,000 and 750,000 m^3 of material but in some cases have showed up to 2,000,000 m^3. These magnitudes are approximate because their real dimensions and geometries are difficult to determine, as these landslides show diffuse boundaries in many cases. Most of the landslides start with creep movements and often evolve into earth flows or complex landslides. There are also examples of translational landslides favoured by the inclined stratification associated to the cuesta-relief.

The city of Loja is experiencing a rapid growth during the last decade covering most of the hilly area located in the bottom of the valley. New urban developments have also been built in the edges of the valley where construction is not advisable because of the poor ground conditions and high slope gradients. Thus, important ground instability problems associated to landslides have emerged with the occupation of these areas and many new neighbourhoods are already experiencing the consequences of their uncontrolled urban development. A review of news and reports about damages caused by landslides in the city of Loja developed during this research reveals that since 2002 to 2013 there had been 46 cases of buildings, roadways or water pipes damaged by mass movements (Fig. 3). Some of the most significant cases are summarized in Table 2.

3. Studied landslides

We identified and mapped 287 landslides in the valley of Loja. Four of these landslides were selected to be characterized in detail. The description of their geological setting, typology, material involved and kinematics should illustrate the most common mass movements in the valley of Loja. The four examples are the landslides of “La Florida”, “El Plateado”, “San Cayetano” y “Chontacruz” (Fig. 4). Tables 3 and 4 show their main characteristics.

3.1. La Florida

On November 13, 2011, an intense rainfall triggered a landslide in “La Florida”, an area located in the NW of the city of Loja. Initially, the activity of the landslide began to be manifested only with some cracks in the ground. Soon after, another intensive rainfall event, occurred on November 28, 2011, reactivated the landslide causing a continuous but very slow creep movement in the slope. Finally, four days later, the landslide evolved in a slow flow that dragged and destroyed 14 buildings. This loss corresponds to the severe damage class according to the damage score system proposed by Cooper (2008).

The mass movement also took out water pipes and power lines causing the disruption of water and electrical services for several days. The landslide provoked damages amounting to 560,000 $. Currently, the landslide is still active and shows a body of 250 m long and 150 m wide. The thickness and the volume of the deposit mobilized were calculated in 20 m and about 750,000 m^3, respectively. We estimate that 40 edifices continue to be at risk because the affected area of the landslide is increasing.

3.2 El Plateado

“El Plateado” is a neighborhood located at the NW of the city of Loja crossed by the Pan-American Highway. Since November 2008, the km, 4 of the stretch between Loja and Catamayo of this famous highway show evidences of deformation: cracks, fissures, settlements in the highway and lobes in the surrounded slope. These features were caused by a creep movement. The creep phenomenon covers an area of 26 ha of a gentle slope and mobilizes only 3.5 m of the surficial deposits. The area of the roadway affected was intensively studied because the importance of this infrastructure and the possible dramatic evolution of this mass movement.

3.2 San Cayetano

Heavy rains for over a week triggered a rapid shallow landslide on Febrary 28, 2012, in the neighborhood of Loja called “San Cayetano Bajo”. The mass movement destroyed one house and caused 56,000 $ in damages. The area affected by the landslide (1.4 ha) show current evidences of instability and we estimate that another 22 houses may be at risk.

3.3 Chontacruz

The landslide of Chontacruz occurred on February 7, 2010, in an area located in the SW of Loja city, after two days of intense rain. The failure started as a rotational slide evolving to a slow flow 220 m long and 48 m wide. This movement caused a significant settlement and horizontal displacement of a roadway and provoked the demolition of a house.

4. Methodology

The landslides have been investigated by combining geophysical, geodetic, geotechnical and mineralogical methods. Geophysical investigation based on Electrical Resistivity Tomography (ERT) were carried out to define accurately the landslide mass. The rates of the shallow movement in the studied landslides were estimated through DGPS monitoring. The geological materials involved in the landslides were characterized according to their geotechnical properties, paying special attention to the mineralogical composition of the clays. Additionally, we performed a precipitation time-series analysis to define the reactivation threshold of each studied landslide.

4.1. DGPS Monitoring

The shallow movement of the four landslides was measured using a GPS monitoring network. This GPS monitoring network consisted of 26 GPS points: 1 reference point and 25 benchmarks. The reference point was the permanent station located in the Campus of the *Universidad Técnica Particular de Loja* (UTPL) that is less than 10 km away from the studied landslides. Figure 5 shows the position of the 25 benchmarks installed in the four study areas. These points include targets adjacent to the active area of each studied landslide, within landslide masses and on potential stable sites. The monitored points consist of concrete landmarks of 50 cm height. Static relative positioning was applied in order to achieve accurate results within an acquisition time of 25 min, 15 s sampling rate and a 10° cut-off angle (e.g. Liu et al. 2005; Sdao et al. 2005; Tagliavini et al. 2007; Abidin et al. 2011; Acar 2010). 4 DGPS campaigns were performed in the four studied landslides between October 2012 and February 2013. Trimble R6 differential GPS equipment was used in all the surveys. One receiver was positioned on a master station, while a rover was moved collecting the data. The data were post-processed using the software Trimble Business Center v.2.2 reaching acceptable accuracy of 0.005 m ± 0.5 ppm. The observations were recorded in the UTM coordinate system, WGS84 datum, Zone 17 S.

4.2. Electrical Resistivity Tomography (ERT)

Eight ERT lines were acquired, two in each landslide: one longitudinal and one transverse to the landslide body, except for "El Plateado" landslide that was covered by two longitudinal ERT lines, one on each side of the Pan-American Highway. Figure 5 shows the location of the ERT profiles. All of them were recorded with a multielectrode Lund system consisting of an ABEM Terrameter SAS4000 used for 2D and 3D high resolution studies with an electrode selector ES464 and a 12 V DC battery. The equipment has a resolution of 25 mV (theoretical, 1 second integration time), three automatic measurement ranges (±250 mV, ±10 V and ± 400 V) and an accuracy of 1% at all temperatures. The data were recorded using a Dipole–Dipole array configuration (ABEM, 2010). Table 5 contains the electrode spacing used in each ETR profile. RES2DINV® ver. 3.59 software was used for the electrical imaging inversion. The best results were obtained applying the robust inversion with maximum errors between 3.0 and 9.2%.

4.3. Geotechnical characterization

The role of geological materials in the formation and dynamics of the landslides was investigated through the analysis of 44 soil samples gathered at a depth of 1–2 m. The location of the samples is shown in Figure 5. The sliding surfaces were characterized by collecting eight samples from the failure plane zone. The moisture content, grain-size analysis and the Atterberg limits were determined in accordance with the ASTM D2216 ASTM D422/00 and ASTM D4318/00 standards, respectively. Cohesion and internal friction angle were established by means of common triaxial UU (Unconsolidated Undrained) conforming to the ASTM D2850 standard.

4.4. Mineralogical analysis of clays

X-ray Diffraction (XRD) was used to determinate mineral composition of the soils involved in landslides. XRD analyses were carried out on both whole unoriented samples and oriented aggregates of the < 2 μm fraction separated by centrifugation (Fig. 6). This study was made in samples collected at different depth of the landslide mass taking special care to characterize relative abundance of smectite clay minerals on the soils. Smectite content in clay soils can control their plasticity, compressibility and swelling pressure (Gillot 1986). The strong interaction between clay minerals and water

results from: a) the high specific surface area of the clay mineral; b) the structure of the clay minerals, and c) the polarity of the water molecule. Smectite identification was corroborated through ethylene-glycol (EGC) and 550º heating treatments (Fig. 6, inset). Ethylene glycol treatment is one of the most widely used methods for identification of 2:1 clay minerals (MacEwan and Wilson 1980; Moore and Reynolds 1997).When a smectite sample is exposed to EGC, H_2O is replaced by this organic substance inducing a shift in the structure and peaks position on XRD (Fig. 6).

4.5. Time-series analysis of precipitation

With the aim to correlate the changes of the triggering factor to the landslide events, a time-series analysis of precipitation in the Loja valley was addressed. For this purpose the data provided by the *Instituto Nacional de Meteorología e Hidrología* and recorded at the "*La Argelia*" meteorological station were used. The data processing involves the following steps:

First, the monthly rainfall for every year of the whole record was taken into account to get the mean precipitation of every month (column "Mean rainfall (mm) (1964-2014)" in Table 6). The driest months were omitted, while all of those closest to the landslides dates were kept. In the same way, the monthly rainfall for every inter-annual period related to each landslide occurrence was adjoined to Table 6. The total rainfall accumulated during every period and their percentage with respect to the mean values, were assessed, so that the first ones can be compared to the latter.

Second, for every landslide dated, the monthly rainfall trend was showed graphically. This consists of plotting the cumulative monthly rainfall for every inter-annual (black continuous line in Figure 7) period together with the mean values expected (black dashed line in Figure 7) (column "Mean rainfall (mm) (1964-2014)" in Table 6). By comparing both curves the rainfall divergence can be easily visualized on the charts. In addition, the percentage of accumulated rainfall with respect to the mean values (red dashed line in Figure 7) was also displayed showing the curve for that divergence.

5. Results

5.1. Landslides kinematics

The GPS monitoring carried out in the four studied landslides provided useful data about kinematics of the studied landslides. All of them except "San Cayetano", can be

described as slow mass movements (Cruden and Varnes 1996). “La Florida”, “El Plateado” and “Chontacruz” landslides show displacement rates of several meters per year, with mean values of 6.8; 3.4 and 4.6 m/yr respectively, whereas "San Cayetano" landslide displays movements of ~0.2 m/yr (Figure 8). It is worth to note that we detect slight movements in adjacent points of the landslides that points out the potential instability of the slopes that surround the sliding area.

The monitoring data reveal that the magnitude of the deformation is distributed homogeneously in the landslide mass of “La Florida”, “San Cayetano” and “Chontacruz” but the deformation in the “El Plateado” tends to concentrate along its right flank. The direction and sense of the measured movements are in accordance with the theoretical expected flow lines inferred from the landslide morphology and the gradient of the slope (Figs. 8 and 9). However, the acquired GPS data show that the displacement rates are not linked to the gradient of the slope. “La Florida” and “El Plateado” landslides show fewer gradients but higher or similar displacement rates than “San Cayetano” and “Chontacruz” landslides. The explanation of this phenomenon lay in the materials involved in this type of landslides and their degree of water saturation. This will be discussed in the following sections that describe in detail the materials and mineralogy of the mobilized mass.

5.2. Geometry and water content of the landslide body

We could infer the geometries and degree of water saturation of the landslide masses on the basis of the stratigraphic data gathered through an exhaustive field survey and ERT profiles (Lapenna et al. 2003). The ERT profiles of "La Florida" clearly reveal two differentiated zones: the lower one with values of resistivity below 6 Ω.m that corresponds to saturated sandy or silty clays; and the upper one, 20 m in thickness, that show values of resistivity in the range of 6 to 80 Ω.m and consist of colluvial deposits with blocks of metamorphic rocks in a silty-clayed matrix. This differentiation is not apparent in the “El Plateado” landslide where there is not a homogeneous variation in the resistivity. The zones that show low resistivity values (~10 Ω.m) are distributed heterogeneously along the two ERT profiles (Fig. 10). In these zones the creep movement is more active and new cracks appeared in the surface because the level of water saturation is very high. The material with the mentioned low resistivity values has been interpreted as saturated sandy or silty clays and the areas with higher values (>22

371 Ω.m) as consolidate sandstone layers. Nonetheless, despite the ERT profiles do not
372 show a clear pattern, a failure plane may be guessed at 10 m deep. The electrical
373 resistivity profiles carried out in the "San Cayetano" and "Chontacruz" landslides show
374 a wide range of resistivity values. We infer from the ERT profiles the sliding plane
375 where a sharp change in the resistivity pattern occurs (Fig. 11). Thus, the approximate
376 depth of this sliding plane is between 10 to 15 m. The low resistivity materials are
377 ascribable to sandy or silty clays as in the previously described landslides. In the case of
378 "San Cayetano" landslide, the high resistivity zones has been attributed to dry sandy
379 clays (15-50 Ω.m) and sandstones (>50 Ω.m). In the "Chontacruz" landslide these zones
380 corresponds to conglomerates of the Quillollaco Fm. The longitudinal ERT profile of
381 "Chontacruz" is very enlightening to know the internal structure of the landslide. The
382 succession of conglomerate and clayey layers in the bedrock can be inferred from the
383 ERT data but the most interesting aspect is that the profile clearly draws how the
384 landslide begins in the clayey units and the material slip over the conglomerates.
385
386 *5.3. Geotechnical and mineralogical characteristics of the geological materials*
387 *involved in the landslides.*
388 Tables 7 and Figure 12 show the main geotechnical characteristics of the samples
389 collected in each landslide. The analyzed landslides show low effective and residual
390 angles of internal friction of 16–28º and 8–12º, respectively. The highest values are
391 related to the presence of silts in the involved materials and the lowest values are
392 associated to high clay content deposits.
393
394 According to Atterberg limits standard (ASTM D4318–00), most of the materials are
395 medium to high plasticity soils (liquid limit LL and plasticity index IP varying in the
396 range 40–91 and 28–58, respectively). The failure plane in the four landslides is
397 associated to layers of silty clays. These clays are high plasticity materials (LL: 59–82
398 and IP: 23–58) with water (moisture) content very close to the plastic limit (Fig. 12 and
399 Table 7).
400
401 The sliding surfaces show a clay-rich layer with high concentration of smectite clay
402 minerals (Fig. 6) as it has been observed in other cases (e.g. Azañón et al. 2010).
403 Smectite on this clay-rich layer is mainly montmorillonite. Small amounts of other clay
404 minerals (kaolinite and illite) and quartz were also found at the base of the landslides.

Montmorillonite is the most expansive clay minerals belong to this group. The high specific surface area is a consequence of the small size and platy shape of this clay mineral grains. The weak ionic bond between filosilicate layers in the structure of the clay, due to the small interlayer charge, allows the bipolar water molecule to dissolve the weakly bonded cations in the interlayer space in proportions highly dependent on water availability. In the case of montmorillonite, the specific surface area is around 760 m^2/g (Yilmaz and Karacan 2002). Thus, smectite-rich clays softened by increased water content can exhibit the properties of a lubricant and can be critical for slope stability. This change in the mechanical properties is of critical importance in understanding the controlling role that smectite-rich layers can represent in the generation of slope failure in areas with low gradients, as in the case of other landslides located in the Loja basin.

5.4. Triggering factor. Rainfall threshold.

Considering the total precipitation of the rainiest period (Sep. – May.) for every study-case, it can be observed that the lower rainfall triggering one of the landslides ("Chontacruz" landslide) reached about 82% of the mean value when considering the whole record 1964-2014 (Table 6). In addition, in two of them ("La Florida & San Cayetano" landslides) the accumulated rainfall reached almost 140% with respect to the mean value, while the cumulative rainfall for "El Plateado" landslide was of about 14% higher than the mean value (Table 6). Within this period, it can be observed several months where the gauged rainfall exceeding 150% with respect to the average value, even one of them overcome the 200% (Sep. - 2011).The curve for the percentage of cumulative rainfall with respect to the mean values for every landslide shows about 180% for the first case (The Florida) (Fig. 7a), about 143% for the second case (San Cayetano) (Fig. 7b), 145% for the third case (The Plateado) (Fig. 7c) and 90% for the last case (Chontacruz) (Fig. 7d).

Summarizing, the landslides dates show as they occurred yearly during 4 consecutive years. Although some months of the rainiest period (Sep. – may.) overcome the 150% of the mean value, the percentage of cumulative rainfall with respect to the mean quantity before every landslide date only reached a maximum of 180% in the first case, while the other three cases occurred after exceeding values between 90% and 145%. Considering the lowest percentage (90%) and the highest value for 3 of the 4 cases (145%), is expected that the cumulative rainfall during the wet period analyzed mean

may trigger landslides with a relative high frequency (near yearly) in the study area. This is a first approximation using only four cases, whereas a larger landslide inventory covering a longer time-interval will be analyzed with the aim of assessing the thresholds and occurrence probability with more accuracy.

6. Discussion

These results allow us to characterize in detail four damaging landslides in Loja Basin. Our observations may also serve as reference for understanding the mechanism and kinematics of the mass movements observed in this basin and in other similar geological settings of Andes. DGPS and ERT measurements combined with a detailed geomorphological evaluation reveal that the studied landslides are of the active slow-moving complex earth-slide earth-flow type (Cruden and Varnes 1996). Geotechnical and mineralogical analysis demonstrated that clay minerals of the smectite group have contributed significantly to the failure and movement in the studied landslides. The high content on these minerals determines how the material involved in the "La Florida" and "El Plateado" landslides show movements with rates up to m/yr in slopes with low gradients (10–15º). On the other hand, the "San Cayetano" landslide present displacement rates of cm/yr although the gradient of the slope is 20º because active clays are less abundant in materials affected by landslides. The observed movements in the "Chontacruz" landslide (4.6 m/yr) can be explained because the high gradient of the slope (40º).

The high montmorillonite content have conferred very high plasticity to the materials involved in the landslides inducing low values in their cohesion and internal friction angles. The great expansive behaviour of the montmorillonite is even enhanced by the tropical climate in the study area. This explain why the studied landslides were developed at hillsides with low gradients (<20º). Previously, Ibadango et al. (2005) had yet determined with a borehole that the failure plain of a landslide, 200 m from the Chontacruz landslide, was developed in strata with high-plasticity clays, therefore, this seems to be a general characteristic of the area.

The montmorillonite is a clay mineral associated to lacustrine sedimentary environments such as the represented by the San Cayetano, Belén and Trigal Formations in Loja Basin. This type of deposits is common in the other Neogene

intramontane basins of Andes which would explain why the landslide phenomena observed in Loja are similar to those described in the Ecuadorian basins of Cuenca, Azogues and Vilcabamba-Malacatos and other places in the Andes where similar lithology is described (see Table 1; PMA, 2007). Thus, characteristics outlined here about the Loja landslides can be used for forecasting in general terms the future behavior of mass movements occurred in the other Andean intramontane basins. Possibly the successful mitigation measures applied in Loja could be also taken as a reference for taking actions against these landslides in the other basins.

The landslide rainfall thresholds calculated through a time-series analysis are coherent with the above mentioned observations. No precipitations far above the mean are required for triggering and reactivating the landslides. This represents a problematic situation with regard to landsliding in the Loja Valley and the other Andean Neogene basins because these areas feature abundant rainfall and high levels of relative moisture. That explains the high number of landslides inventoried in the Loja Valley that cause repetitive damages in the infrastructures and urban areas. Therefore, the production of a sound landslide hazard map of these areas should be a priority to support land planning. The results of this research will help in this task.

The research conducted on the four studied landslides has also provided valuable information on the future evolution of the studied mass movements for avoiding new damages. DGPS measurements revealed precursory movements coherent with the landslide displacement outside of the identified landslides bodies. This is indicative of future landslide progression and has important risk management implications. Emergency or evacuation measures can be carried out before a catastrophic movement occur in the area where we detected previous displacements. On the other hand, the gathered data will be used for modelling numerically these landslides: (1) DGPS displacements and rainfall thresholds will be used for calibrating the models; (2) ERT profiles will serve to define the geometry and water content of the landslide bodies; and (3) geotechnical and mineralogical analyses will be used to characterize the involved materials. We can design appropriate and optimized mitigation measures by simulating different alternatives by means of numerical models.

The presented methodology may be a reference for performing new landslide characterizations for avoiding future losses in the Andean region. ERT and DGPS provide a quick and low-cost diagnosis of the instability situation for taking rapid decisions regarding the risk management. Geotechnical and mineralogical characterization and the rainfall threshold analysis serve to forecast the future evolution of a landslide and to pose suitable mitigation measures. Additionally, the conceptual model derived from the studied landslides may be applied to better understand the mass movements described in other Andean intramontane basins (Table 1). These basins usually correspond with wide valleys where important cities are situated such as Tulúa, Bugá, Cartago or Bogotá in Colombia; Cuenca, Azogues, Riobamba or Latacunga in Ecuador; Cajamarca, Huancayo, Cusco or Ayacucho in Perú; and Cochabamba or La Paz in Bolivia. All these cities have sectors that are growing in landslide-prone areas as is the case of Loja. This creates remarkable landslide risk situations as reflected by the damages shown in Table 4 The knowledge gathered during this research and the presented procedure can be used to avoid or minimize most of these damages.

7. Conclusions

The comprehensive study of four landslides occurred in Loja (Ecuador) have served to formulate a detailed conceptual model of the common landslides that occur in this area. These landslides are slow mass movements but, according to DGPS measurements, three of them show considerable velocities regarding to their damage potential (around ~3–7 m/yr). Although the size of the landslides can be considered medium, the analyzed movements are mainly surficial as ERT profiles show. Geotechnical and mineralogical analyses demonstrate that the main causal factor is the presence of active clay minerals in the involved geological formations. These clays explain why low gradient slopes failed after precipitation periods not exceptionally intensive.

All this information obtained through the integration of several techniques significantly contributes to the understanding of the movements observed in Loja. Now, physical models can be developed to forecast the behavior of the analyzed movements and design optimized mitigation measures for avoiding future losses. The conceptual model can also help in the production of a landslide susceptibility map for managing properly the urban development in Loja city. Owing to lack of international publications about comprehensive analysis of landslides integrating different techniques in the Andean

region, this study serve as a reference for future studies and for understanding similar cases occurred in this region.

Acknowledgements

This PhD study is supported through a grant awarded by the Ministry of Higher Education, Science, Technology and Innovation (SENESCYT) under the scholarship program "Open Call 2012 Second Phase" of the government of Ecuador. We thank Diego Jara and Daniel Bravo for field assistance. J.P. Galve acknowledges funding by the Spanish Ministry of Economy and Competitiveness through the 'Juan de la Cierva' Programme.

References

ABEM (2010) Instruction Manual Terrameter SAS 4000/SAS 1000. ABEM Instrument AB, Sundbyberg, Sweden (148 pp.)

Abidin HZ, Andreas H, Gumilar I, Fukuda Y, Pohan YE, Deguchi T (2011) Land subsidence of Jakarta (Indonesia) and its relation with urban development. Nat Hazards 59:1753–1771. doi: 10.1007/s11069-011-9866-9

Acar M, Ozludemir MT, Erol S, Celik R, Ayan T (2008) Kinematic landslide monitoring with Kalman filtering. Nat Hazards Earth Syst Sci 8:213–221. doi: 10.5194/nhess-8-213-2008

Acar M (2010) Determination of strain accumulation in landslide areas with GPS measurements. Sci Res Essays 5:763–768.

Azañón JM, Azor A, Yesares J, Tsige M, Mateos RM, Nieto F, Delgado J, López-Chicano M, Martín W, Rodríguez-Fernández J (2010) Regional-scale high-plasticity clay-bearing formation as controlling factor on landslides in Southeast Spain. Geomorphology 120:26–37. doi: 10.1016/j.geomorph.2009.09.012

Brückl E, Brunner FK, Kraus K (2006) Kinematics of a deep-seated landslide derived from photogrammetric, GPS and geophysical data. Eng Geol 88:149–159. doi: 10.1016/j.enggeo.2006.09.004

Calcaterra S, Cesi C, Di Maio C, Gambino P, Merli K, Vallario M, Vassallo R (2012) Surface displacements of two landslides evaluated by GPS and inclinometer systems: A case study in Southern Apennines, Italy. Nat Hazards 61:257–266. doi: 10.1007/s11069-010-9633-3

Colangelo G, Lapenna V, Loperte A, Perrone A, Telesca L (2008) 2D electrical resistivity tomographies for investigating recent activation landslides in Basilicata Region (Southern Italy). Ann Geophys 51:275–285.

576 Colangelo G, Perrone A (2012) Geoelectrical tomography as an operative tool for
577 emergency management of landslide: An application in basilicata region, Italy. Int
578 J Geophys. doi: 10.1155/2012/593268

579 Coltorti M, Brogi A, Fabbrini L, Firuzabadì D, Pieranni L (2011) The sagging deep-
580 seated gravitational movements on the eastern side of Mt. Amiata (Tuscany, Italy).
581 Nat Hazards 59:191–208. doi: 10.1007/s11069-011-9746-3

582 Cooper A (2008) The classification, recording, databasing and use of information about
583 building damage caused by subsidence and landslides. Q J Eng Geol Hydrogeol
584 41:409–424. doi: 10.1144/1470-9236/07-223

585 Cruden DM, Varnes DJ (1996) Landslide types and processes. In: Turner AK, Schuster
586 RL (eds) Landslides: investigation and mitigation. Special Report 247:36–75

587 Dogan U, Oz D, Ergintav S (2013) Kinematics of landslide estimated by repeated GPS
588 measurements in the Avcilar region of Istanbul, Turkey. Stud Geophys Geod
589 57:217–232. doi: 10.1007/s11200-012-1147-x

590 Galindo-Zaldívar J, Soto J, Ruano P, Tamay J, Lamas F, Guartán J, Azañón JM,
591 Paladines A (2010) Geometría y estructuras de la cuenca neógena de Loja a partir
592 de datos gravimétricos (Andes Ecuatorianos). Geogaceta 48:215–218.

593 Garrido J, Delgado J (2013) A recent, retrogressive, complex earthflow-earth slide at
594 Cenes de la Vega, southern Spain. Landslides 10:83–89. doi: 10.1007/s10346-012-
595 0358-0

596 Gili JA, Corominas J, Rius J (2000) Using global positioning system techniques in
597 landslide monitoring. Eng Geol 55:167–192.

598 Gillot EJ (1986) Some clay-related problems in engineering geology in North America.
599 Clay Minerals. 21:261–278.

600 Giordan D, Allasia P, Manconi A, Baldo M, Santangelo M, Cardinali M, Corazza A,
601 Albanese V, Lollino G, Guzzetti F (2013) Morphological and kinematic evolution
602 of a large earthflow: The Montaguto landslide, southern Italy. Geomorphology
603 187:61–79. doi: 10.1016/j.geomorph.2012.12.035

604 Grana V, Tommasi P (2014) A deep-seated slow movement controlled by structural
605 setting in marly formations of Central Italy. Landslides 11:195–212. doi:
606 10.1007/s10346-013-0384-6

607 Hibert C, Grandjean G, Bitri A, Travelletti J, Malet JP (2012) Characterizing landslides
608 through geophysical data fusion: Example of the La Valette landslide (France).
609 Eng Geol 128:23–29. doi: 10.1016/j.enggeo.2011.05.001

610 Hungerbühler D, Steinmann M, Winkler W, Sewards D, Egüez A, Peterson DE, Helg
611 U, Hammer C (2002) Neogene stratigraphy and Andean geodynamics of southern
612 Ecuador. Earth-Science Rev 57:75–124. doi: 10.1016/S0012-8252(01)00071-X

613 Ibadango C, Soto J, Tamay J, Escudero P, Porter M (2005) Mass movements in the Loja
614 Basin- Ecuador, South America. Proceedings, Int Conf Landslide Risk
615 Management. Vancouver, Canada. 10:1 – 7.

616 Instituto Nacional de Investigación Geológico Minero y Metalúrgio (INIGEMM),
617 (2013). Mapa de susceptibilidad por movimientos en masa del Ecuador, escala
618 1:1,000,000. Technical report. Unpublished.

619 Irigaray C, Lamas F, El Hamdouni R, Fernández T, Chacón J (2000) The Importance of
620 the Precipitation and the Susceptibility of the Slopes for the Triggering of
621 Landslides Along the Roads. Nat Hazards 21:65–81. doi:
622 10.1023/A:1008126113789

623 Irigaray C, Palenzuela JA (2013) Análisis de la actividad de movimientos de ladera
624 mediante láser escáner terrestre en el suroeste de la Cordillera Bética (España)
625 Landslide activity analysis using terrestrial laser scanning at southwest of the Betic
626 Cordillera (Spain). Revista de Geología Aplicada a la Ingeniería y al Ambiente
627 31:53–67.

628 Kennerley JB (1980) Outline of the geology of Ecuador. Overseas Geology Mineral
629 Resources 55:17.

630 Lapenna V, Lorenzo P, Perrone A, Piscitelli S, Rizzo E, Sdao F (2003) High-resolution
631 geolectrical tomographies in the study of Giarrossa landslide (southern Italy). Bull
632 Eng Geol Environ 62:259–268. doi: 10.1007/s10064-002-0184-z

633 Lapenna, V., Lorenzo, P., Perrone, A., Piscitelli, S., Rizzo, E., Sdao F (2005) 2D
634 electrical resistivity imaging of some complex landslides in Lucanian Apennine
635 chain, southern Italy. Geophysics 70:11–18. doi: 10.1190/1.1926571

636 Litherland M, Aspden JA, Jemielita RA (1994) The metamorphic belts of Ecuador.
637 British Geological Survey 11:147

638 Liu GY, Zhu YZ, Zhou RS (2005) A new approach of single epoch GPS positioning for
639 landslide monitoring. Acta seismologica sínica, 18:427–434. doi: 10.1007/s11589-
640 005-0020-1

641 Malet JP, Maquaire O, Calais E (2002) The use of Global Positioning System
642 techniques for the continuous monitoring of landslides: application to the Super-
643 Sauze earthflow (Alpes-de-Haute-Provence, France).Geomorphology 43:33–54.

644 MacEwan DM, Wilson MJ (1980) Interlayer and intercalation complexes of clay
645 minerals. Crystal structures of clay minerals and their X-ray identification, 5, 197-
646 248.

647 Marocco R, Eguez A, Lavenu A, Noblet C, Baudino R, Winter T (1994). Las cuencas
648 intramontanosas neogenas del Ecuador. Resúmenes de conferencias ORSTOM
649 (Ecuador). Ediciones ORSTOM, Quito, Ecuador, 135-138.

Mora P, Baldi P, Casula G, Fabris M, Ghirotti M, Mazzinie E, Pesci A (2003) Global Positioning Systems and digital photogrammetry for the monitoring of mass movements: application to the Ca'di Malta landslide (northern Apennines, Italy). Eng Geol 68:103–121.

Moore DM, Reynolds RC (1997) X-Ray diffraction and the identification and analysis of clay minerals, 2nd. (Vol. 378). Oxford: Oxford university press.

Noferini L, Pieraccini M, Mecatti D, Macaluso, G., Atzeni, C., Mantovani, M, Marcato G, Pasuto A, Silvano S, Tagliavini F (2007) Using GB-SAR technique to monitor slow moving landslide. Eng Geol 95:88–98. doi: 10.1016/j.enggeo.2007.09.002

Palenzuela JA, Jiménez-Perálvarez JD, El Hamdouni R, Alameda-Hernández P, Chacón J, Irigaray C (2015) Integration of LiDAR data for the assessment of activity in diachronic landslides: a case study in the Betic Cordillera (Spain). Landslides. doi: 10.1007/s10346-015-0598-x

Perrone A, Lapenna V, Piscitelli S (2014) Electrical resistivity tomography technique for landslide investigation: A review. Earth-Science Rev 135:65–82. doi: 10.1016/j.earscirev.2014.04.002

Petley D (2012) Global patterns of loss of life from landslides. Geology 40:927–930. doi: 10.1130/G33217.1

Proyecto Multinacional Andino (PMA): Geociencias para las Comunidades Andinas (2007) Movimientos en masa en la Región Andina: Una guía para la evaluación de amenazas. Servicio Nacional de Geología y Minería, Publicación Geológica Multinacional, No. 4, 432 p., 1 cd-rom.

Rizzo V (2002) GPS monitoring and new data on slope movements in the Maratea Valley (Potenza, Basilicata). Phys Chem Earth 27:1535–1544. doi: 10.1016/S1474-7065(02)00174-2

Sdao F, Pascale S, Rutigliano P (2005) Geomorphological features and monitoring of a large and complex landslide near Avigliano urban area (South Italy). Adv Geosci 2:97–101. doi: 10.5194/adgeo-2-97-2005

Tagliavini F, Mantovani M, Marcato G, Pasuto A, Silvano S (2007) Validation of landslide hazard assessment by means of GPS monitoring technique – a case study in the Dolomites (Eastern Alps, Italy). Nat Hazards Earth Syst Sci 7:185–193. doi: 10.5194/nhess-7-185-2007

Travelletti J, Malet JP, Hibert C, Grandjean G (2009) Integration of geomorphological, geophysical and geotechnical data to define the 3D morpho-structure of the La Valette mudslide, Ubaye Valley, French Alps. Proc Int Conf Landslide Process from geomorpho- Log Mapp to Dyn Model 203–208.

687 Yilmaz I, Karacan E (2002) A Landslide in Clayey Soils: An Example from the
688 Kızıldag Region of the Sivas-Erzincan Highway (Sivas-Turkey). *Environmental*
689 *Geosciences*, *9*(1), 35-42.
690

691 Zárate B (2011) Monitoreo de movimientos de ladera en el sector de San Pedro de
692 Vilcabamba mediante procedimientos GPS. Maskana 2:17–25.

693 Zhou P, Zhou B, Guo J, Li D, Ding Z, Feng Y (2005) A Demonstrative GPS-aided
694 Automatic Landslide Monitoring System in Sichuan Province. J Glob Position Syst
695 4:184–191. doi: 10.5081/jgps.4.1.184

696
697
698

TABLES

Table 1. Characteristics of published landslides in the Andean region (simplified PMA, 2007). Dz: slide, R: rotational, T: translational, F: flow; EF: earth flow, Cm: complex, M: Coll: colluvial, GP: Gravels, CL: clays, ML: silts, SM: sands, DVM: volcano sedimentary deposits, Met: metamorphic, Cog: conglomerated.

ID	Case-site	Tipology	Country	Lithology	depth	Trigger	Damage
A4	Freeway Caracas-La Guaira	Dz	Venezuela	Coll	s/d	Seism	affected bridge
A5	San Isidro (La Paz)	R	Bolivia	CL, ML, SM, Cog.	25	water infiltration	Homes affected
A6	Paccha-Achupallas (Chimborazo)	R	Ecuador	DVM	9	irrigation water	Homes affected
A7	Cuarto Centenario (La Paz)	R	Bolivia	GP, CL, ML, SM.	55	Rainfall, irrigation water	Housing and roads
A8	Río San Pedro (Los Lagos)	R	Chile	CL/Met.	80	Seism	River damming
A9	Huamancharpa (Cusco)	T	Perú	SM, Shales	s/d	Rainfall	Any
A10	Mayunmarca	T/F	Perú	SM, Shales, Cog, /Met.	150	water infiltration	600 deads, homes and roads
A12	Cerro Pucaloma (La Paz)	T	Bolivia	Cog, /Met.	s/d	Rainfall, mining	69 deads, 300 homes
A13	Valle de Allpacoma (La Paz)	T	Bolivia	CL, ML, SM.	110	Litología y pendiente	River damming
A14	Ravine de la Troya (La Rioja)	T	Argentina	SM, Shales	6	Rainfall, seism	s/d
A16	Auyos y Asia (Pataz)	Cm/F	Perú	Coll/Cog. SM.	s/d	water infiltration	roads
A17	La Josefina (Azuay)	F	Ecuador	Cog, SM/Met.	80	Rainfall, Based cut slope	Homes, crops , roads, power plant , railway line
A18	Villatina (Medellín)	EF	Colombia	CL, ML	6	Rainfall, irrigation water	450 deads, homes
A19	River Limón (Maracay, Aragua)	F	Venezuela	Detritus, Coll.	1.5	Rainfall	deads, 1500 homes, vehicles, 3 bridges
A20	San Carlos (Antioquia)	M	Colombia	CL, ML, SM.	s/d	Rainfall, seism	20 deads, 27 homes, roads
A24	San Cayetano (Cundinamarca)	EF	Colombia	Coll/Shales, ML, SM.	s/d	Rainfall	homes, 180 families evacuated

Table 2. Summary of some cases histories with direct damage

Case site	Date	Damage	Cause	Economic estimation of damage ($)
Neighborhood "Reinaldo Espinoza"	abr-92	2 houses destroyed	Rainfall	80,000
School "Adolfo Valarezo"	jun-99	1 building cracked, bleachers of basketball court, brickwork	Rainfall	200,000
School "27 de Febrero"	nov-99	brickwork, sports space and toilets	Rainfall	25,000
UV Televisión	nov-99	courtyard and street	Rainfall	50,000
Neighborhood "La Florida"	13/11/2011	14 houses destroyed and 40 at risk	Rainfall	560,000
Neighborhood "La Banda"	09/02/2013	3 houses destroyed, 180 cracked, and via damaged	Rainfall	800,000
Street Villonaco, Obra Pía	01/11/2007	2 houses destroyed and 1 fatalities	Rainfall	60,000
Chirimoyo, Salapa alto	23/06/2007	Tubing water city	Rainfall	5,000
Sierra Nevada	26/03/2015	1 house and 6 fatalities	Rainfall	20,000

Table 3. Summary and monitors the occurrence of landslides analyzed

Case	Localization	Displacement, measurement method	Duration of monitoring months	Slope	Trigger	date of occurrence
1	La Florida	Differential GPS	4	15°	Rainfall	13 nov-11
2	El Plateado	Differential GPS	4	10°	Rainfall-anthropic activities	02 nov-08
3	San Cayetano	Differential GPS	4	20°	Rainfall	feb-12
4	Chontacruz	Differential GPS	4	40°	Rainfall	feb-10

Table 4. Summary of the characteristics and damage from landslides analyzed

Case	Movement rate (mm/year)	Material de rupture surface	Tipology	depth fault plane (m)	Displaced mass (m^3)	Damage	Vulnerability
1	6840	Plastic clay, silty clays	Complex (translation-flow)	30	750000	14 houses	40 houses
2	3430	Plastic clay	Creeping	3.5	63502	Avenue Panamericana towards Catamayo	10 houses and avenue
3	174	clays and silts	Flow	3.2	15393	2 houses	22 houses
4	4630	clays and silts	Creeping-flow	10	105600	1 house, concrete basketball area, road damage	10 houses

Table 5. Electrode spacing used in each ETR profile

Landslide	ETR profile	No. Electrode	Electrode spacing (m)	Total length (m)
Florida	A - A´	72	5	360
	B - B´	72	2	144
Plateado	A - A´	76	3	228
	B - B´	76	3	228
San Cayetano	A - A´	72	3.5	252
	B - B´	72	2	144
Chontacruz	A - A´	70	3	210
	B - B´	74	2	148

747

748 **Table 6.** Cumulative and total rainfall for the rainiest period covering the months from
749 September to may

750

Month	Cumulative rainfall for the mean values of the months Sep. to May (mm) (1964-2014)	Percentage of cumulative rainfall for the interval Sep. - May (%) for every study-case		
		Plateado	Chontacruz	Florida & San Cayetano
		2008-2009	2009-2010	2011-2012
September	43.36	47.51	128.22	207.09
October	115.55	188.94	96.55	112.06
November	182.73	153.18	38.7	232.08
December	268.09	147.96	138.71	191.78
January	358.86	146.53	65.44	161.95
February	483.57	72.33	87.88	161.65
March	619.98	98.52	33.94	44.35
April	713.64	99.4	80.93	104.42
May	774.6	71.04	115.99	134.7
Mean total rainfall for Sept. - May (mm):	774.6	880.2	631.5	1079.3
% related to the mean total rainfall for Sep. - May (774,6 mm):		113.63	81.53	139.33

751
752

753

754 **Table 7.** Geotechnical properties of the materials involved in the slip plane

Geotechnical characteristics	La Florida	El Plateado	San Cayetano	Chontacruz
Liquid limit	82	72	59	69
Plastic limit	31	29	36	32
Plastic index	51	43	23	37
Moisture content	24.5%	34.0%	35.2%	37.5%
Consistency index	1.13	0.88	1.03	0.85
Cohesion	157 kPa	39 kPa	88 kPa	127 kPa
Effective angle of internal friction	16º	20º	22º	28°
Residual angle of internal friction	9º	12º	8º	--
Specific gravity	1.8	1.9	1.9	1.8
Analysis number	**2**	**2**	**2**	**2**

755

756

757

758

FIGURE CAPTIONS

Figure 1. a) Map of South America with published examples of landslides developed in silty clays (Modifiedfrom PMA, 2007). b) Location of intramontane Neogene basins of Ecuador. Ch: Chota; G: Guayabamba; L: Latacunga; R: Riobamba; C: Cuenca; Gi: Girón; N: Nabón; Lo: Loja; V: Vilcabamba-Malacatos; Z: Zumba (modified from Marocco et al., 1994). c) Landslide inventory map of Ecuador (modified from INIGEMM, 2013).

Figure 2. Location sketch of the studied area, simplified geological map and the four studied cases are indicated in yellow circles.

Figure 3. Number of slides with direct damage (2002-2013) in Loja. Source: Journal "La Hora" and "El Comercio"

Figure 4. Photographs of the damage caused by the studied landslides.

Figure 5. Location of seismic and ERT profiles, DGPS points, soil samples in each investigation site.

Figure 6. XRD clay samples, showing that the smectite is dominant clay mineral. (b2μm clay fraction, glycolated sample and 100 °C-heated sample difractograms).

Figure 7. Cumulative rainfall for the rainiest period affecting each studied landslide

Figure 8. Vector distribution indicating the estimated annual velocity.

Figure 9. Geological map of the studied cases: **a**) The Florida **b**) The Plateado **c**) San Cayetano **d**) Chontacruz; and location of the geological sections (C-C`; D-D`; E-E`; F-F`) showed in Figure 11.

Figure 10. Analysis of longitudinal and transverse ERT profiles, and its correlation with the geological section. **a**) case "La Florida", **b**) case "El Plateado".

Figure 11. Analysis of longitudinal and transverse ERT profiles, and its correlation with the geological section. **c**) case "San Cayetano", **d**) case "Chontaccruz".

Figure 12. Location of the 44 studied samples in the Casagrande plasticity chart. The materials of the failure planes are represented by grey circles.

Figure 1

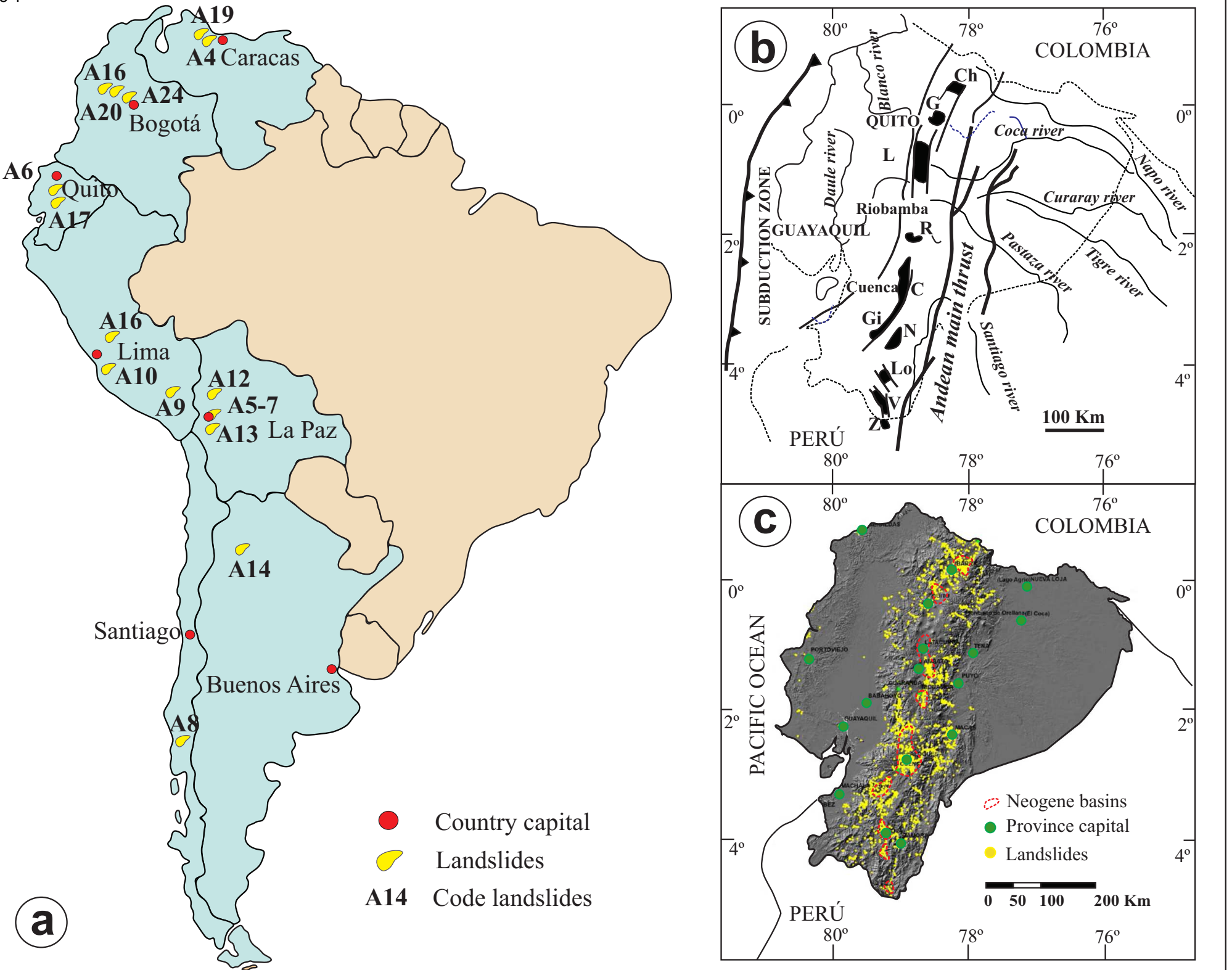
a
A19
A4 Caracas
A16
A24
A20
Bogotá
A6
Quito
A17
A16
Lima
A10
A9
A12
A5-7
A13 La Paz
A14
Santiago
Buenos Aires
A8
Country capital
Landslides
A14 Code landslides
b
COLOMBIA
PERÚ
SUBDUCTION ZONE
GUAYAQUIL
QUITO
Riobamba
Cuenca
Blanco river
Daule river
Coca river
Napo river
Curaray river
Pastaza river
Tigre river
Santiago river
Andean main thrust
Ch
G
L
R
C
Gi
N
Lo
V
Z
100 Km
c
COLOMBIA
PERÚ
PACIFIC OCEAN
Neogene basins
Province capital
Landslides
0 50 100 200 Km
80º
78º
76º
0º
2º
4º

Figure 2

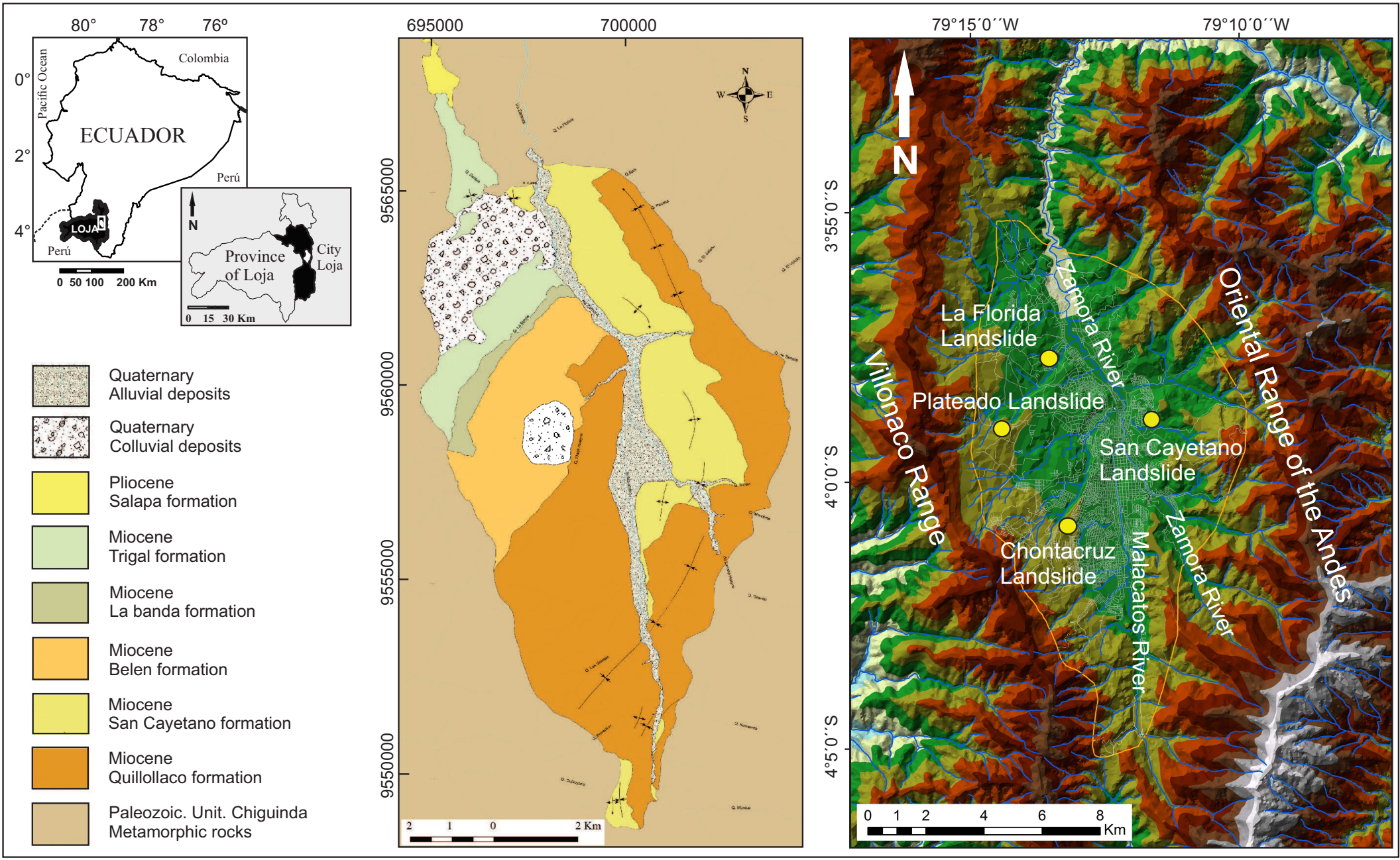
80°
78°
76°
0°
2°
4°
Pacific Ocean
Colombia
ECUADOR
Perú
LOJA
Perú
0 50 100 200 Km
N
Province of Loja
City Loja
0 15 30 Km
Quaternary Alluvial deposits
Quaternary Colluvial deposits
Pliocene Salapa formation
Miocene Trigal formation
Miocene La banda formation
Miocene Belen formation
Miocene San Cayetano formation
Miocene Quillollaco formation
Paleozoic. Unit. Chiguinda Metamorphic rocks
695000
700000
9565000
9560000
9555000
9550000
N
W
E
S
2 1 0 2 Km
79°15´0´´W
79°10´0´´W
3°55´0´´S
4°0´0´´S
4°5´0´´S
N
La Florida Landslide
Plateado Landslide
San Cayetano Landslide
Chontacruz Landslide
Villonaco Range
Zamora River
Oriental Range of the Andes
Malacatos River
Zamora River
0 1 2 4 6 8 Km

Figure 3

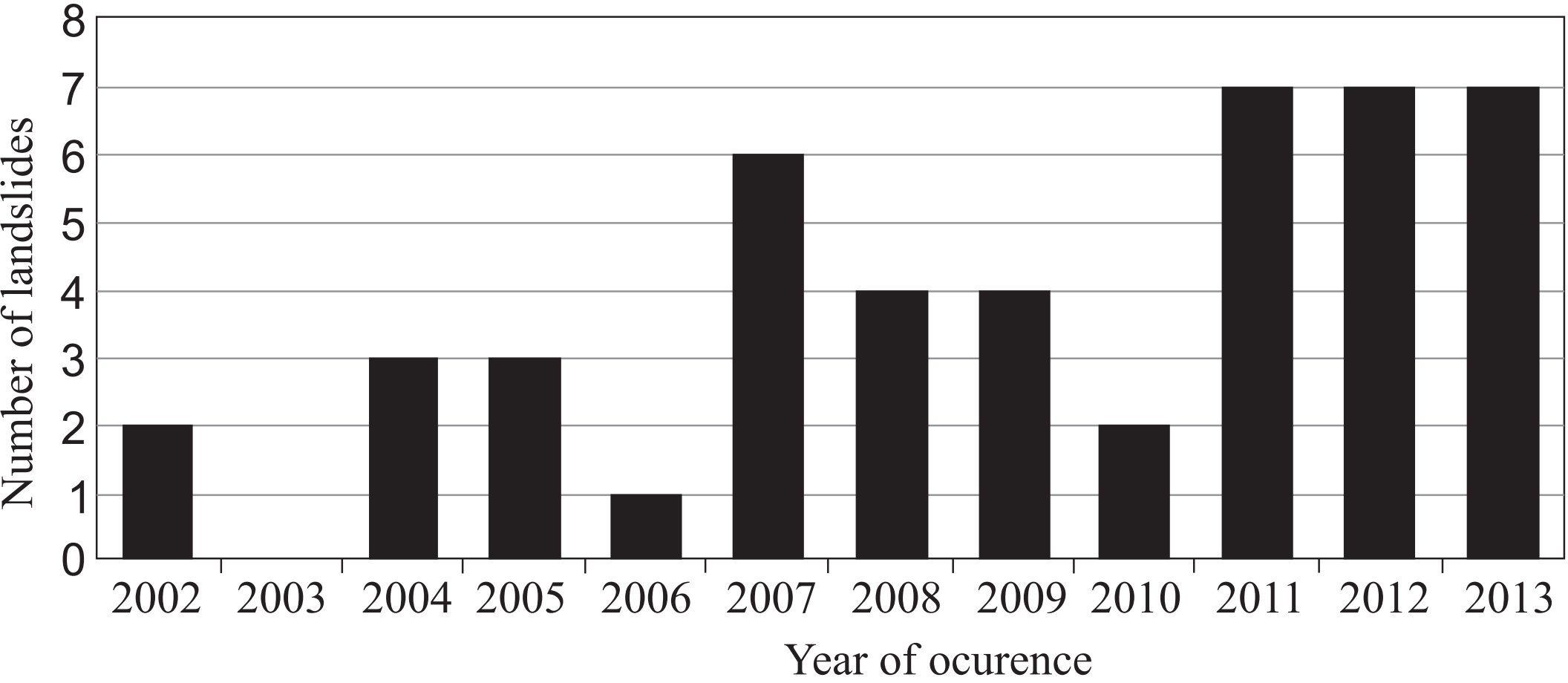
Number of landslides
0
1
2
3
4
5
6
7
8
2002
2003
2004
2005
2006
2007
2008
2009
2010
2011
2012
2013
Year of ocurence

Figure 4

Click here to download Figure Fig4.eps

Figure 5

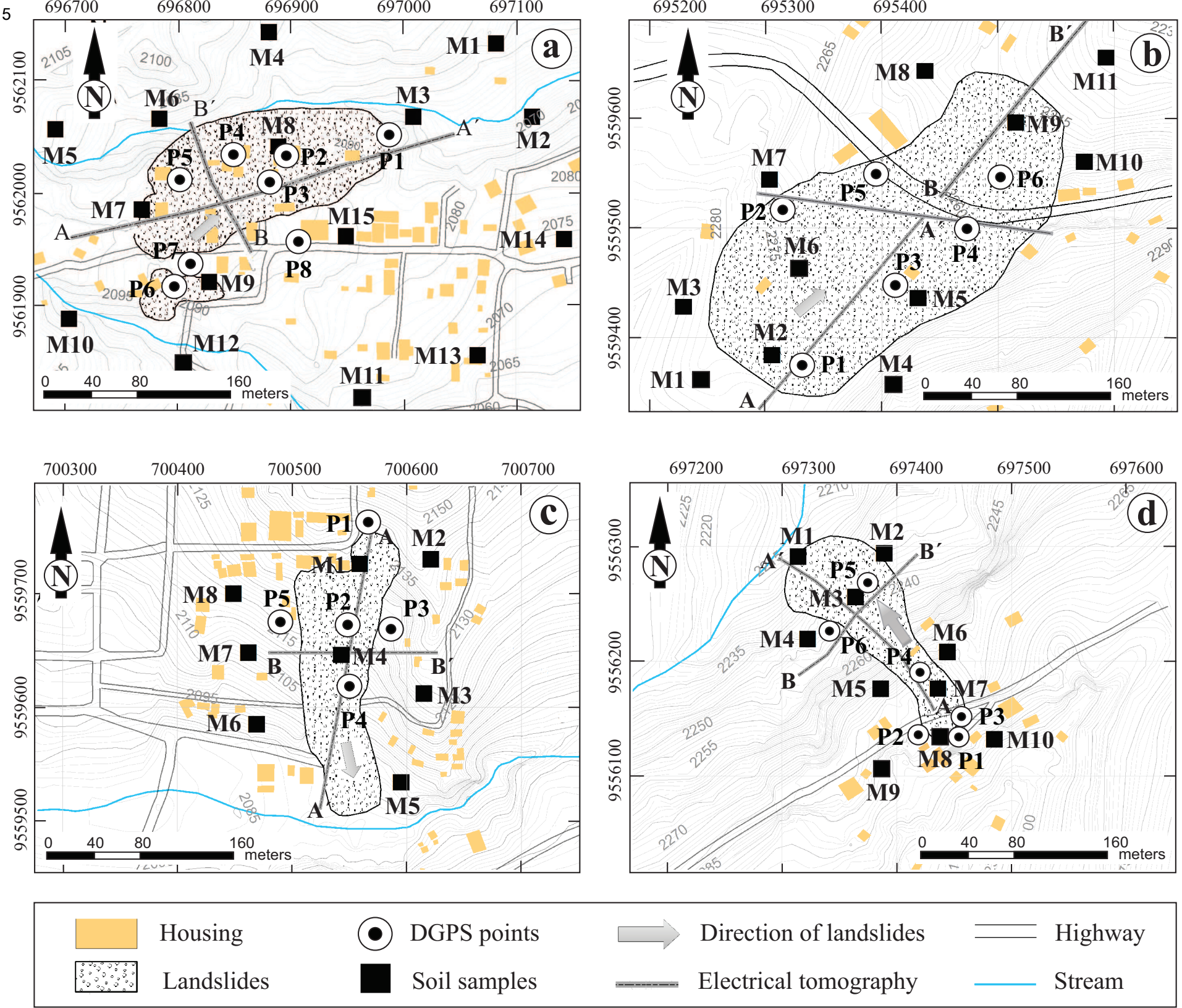
a
b
c
d
N
meters
0 40 80 160
Housing
Landslides
DGPS points
Soil samples
Direction of landslides
Electrical tomography
Highway
Stream

Figure 6

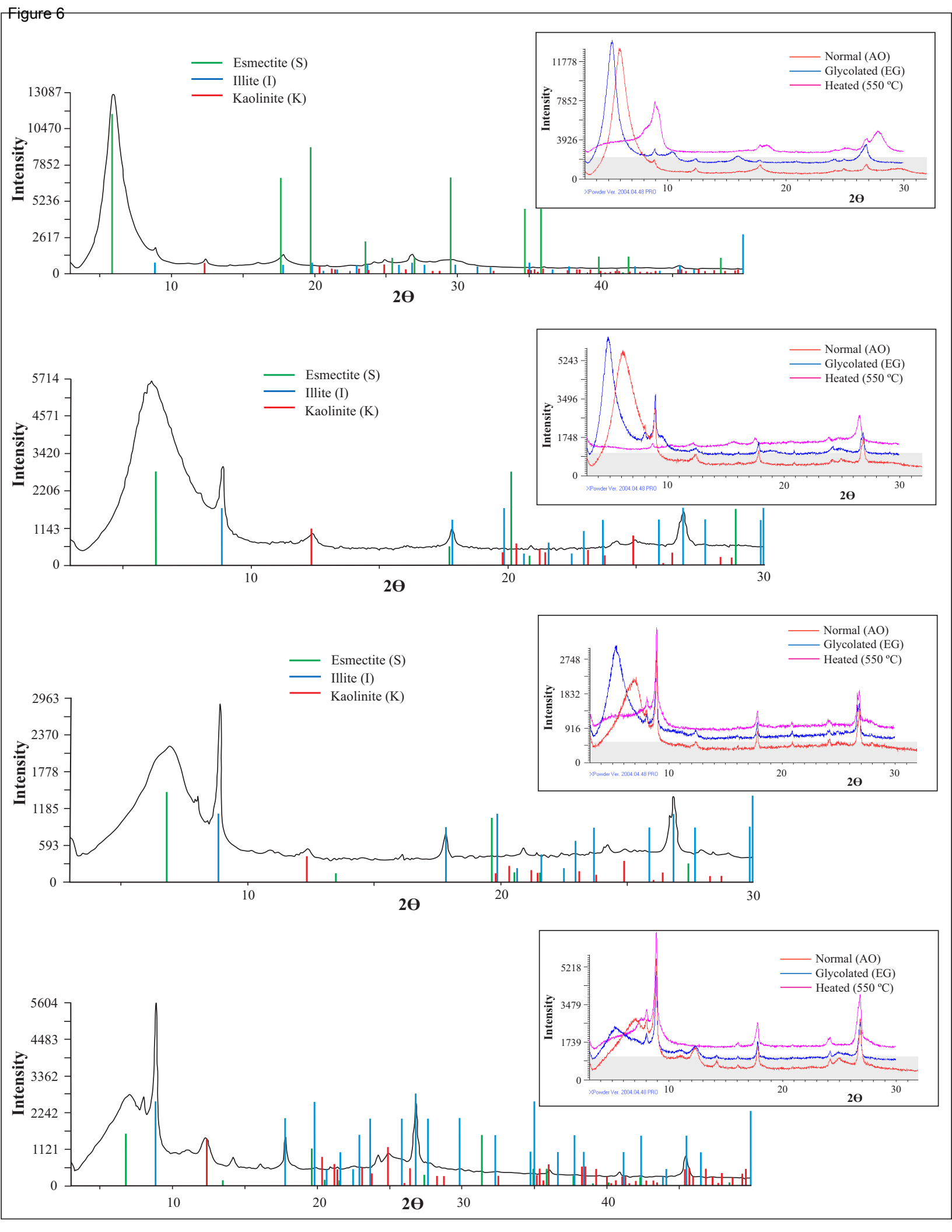
Esmectite (S)
Illite (I)
Kaolinite (K)
Intensity
2Θ
Normal (AO)
Glycolated (EG)
Heated (550 ºC)
XPowder Ver. 2004.04.48 PRO

Figure 7

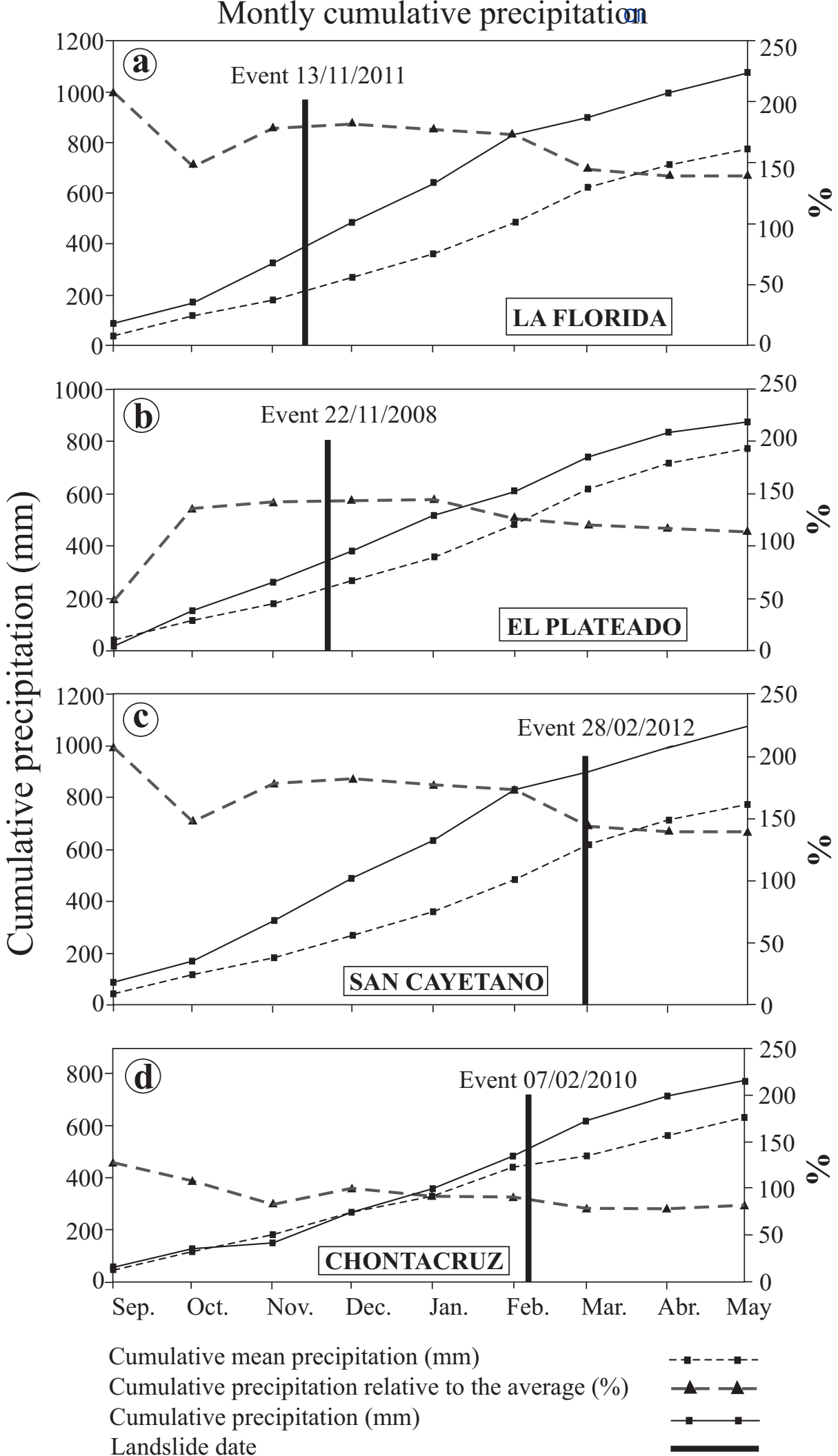
Montly cumulative precipitation
a
Event 13/11/2011
LA FLORIDA
b
Event 22/11/2008
EL PLATEADO
c
Event 28/02/2012
SAN CAYETANO
d
Event 07/02/2010
CHONTACRUZ
Cumulative precipitation (mm)
%
Sep.
Oct.
Nov.
Dec.
Jan.
Feb.
Mar.
Abr.
May
Cumulative mean precipitation (mm)
Cumulative precipitation relative to the average (%)
Cumulative precipitation (mm)
Landslide date

Figure 8

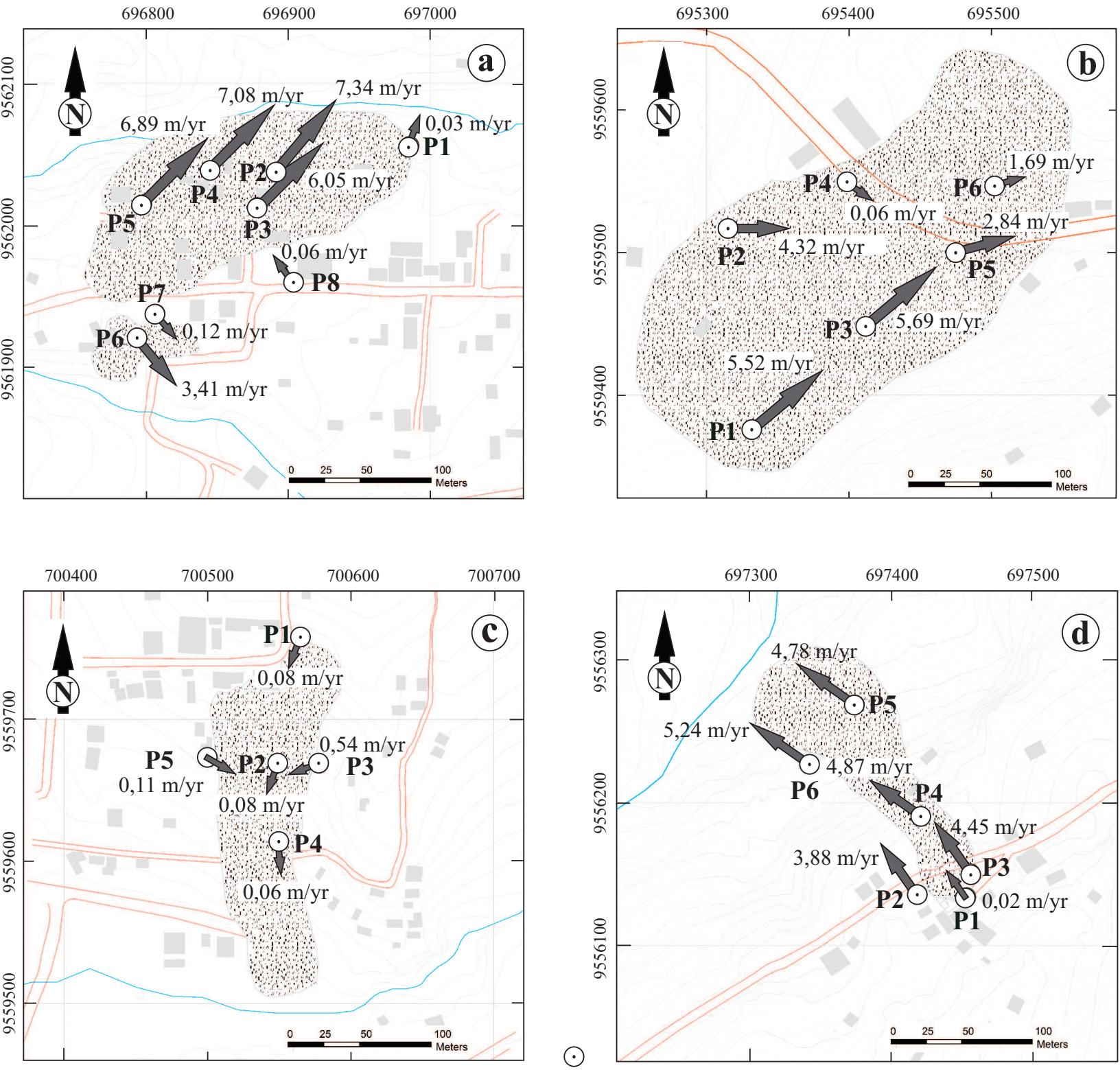
a
696800
696900
697000
9562100
9562000
9561900
N
7,08 m/yr
7,34 m/yr
6,89 m/yr
0,03 m/yr
P1
P2
P4
6,05 m/yr
P5
P3
0,06 m/yr
P8
P7
0,12 m/yr
P6
3,41 m/yr
0 25 50 100
Meters
b
695300
695400
695500
9559600
9559500
9559400
N
1,69 m/yr
P4
P6
0,06 m/yr
2,84 m/yr
P2
4,32 m/yr
P5
P3
5,69 m/yr
5,52 m/yr
P1
0 25 50 100
Meters
c
700400
700500
700600
700700
9559700
9559600
9559500
N
P1
0,08 m/yr
0,54 m/yr
P5
P2
P3
0,11 m/yr
0,08 m/yr
P4
0,06 m/yr
0 25 50 100
Meters
d
697300
697400
697500
9556300
9556200
9556100
N
4,78 m/yr
P5
5,24 m/yr
4,87 m/yr
P6
P4
4,45 m/yr
3,88 m/yr
P3
P2
0,02 m/yr
P1
0 25 50 100
Meters
Housing
Landslides
DGPS points
Displacement vector
Highway
Stream

Figure 9

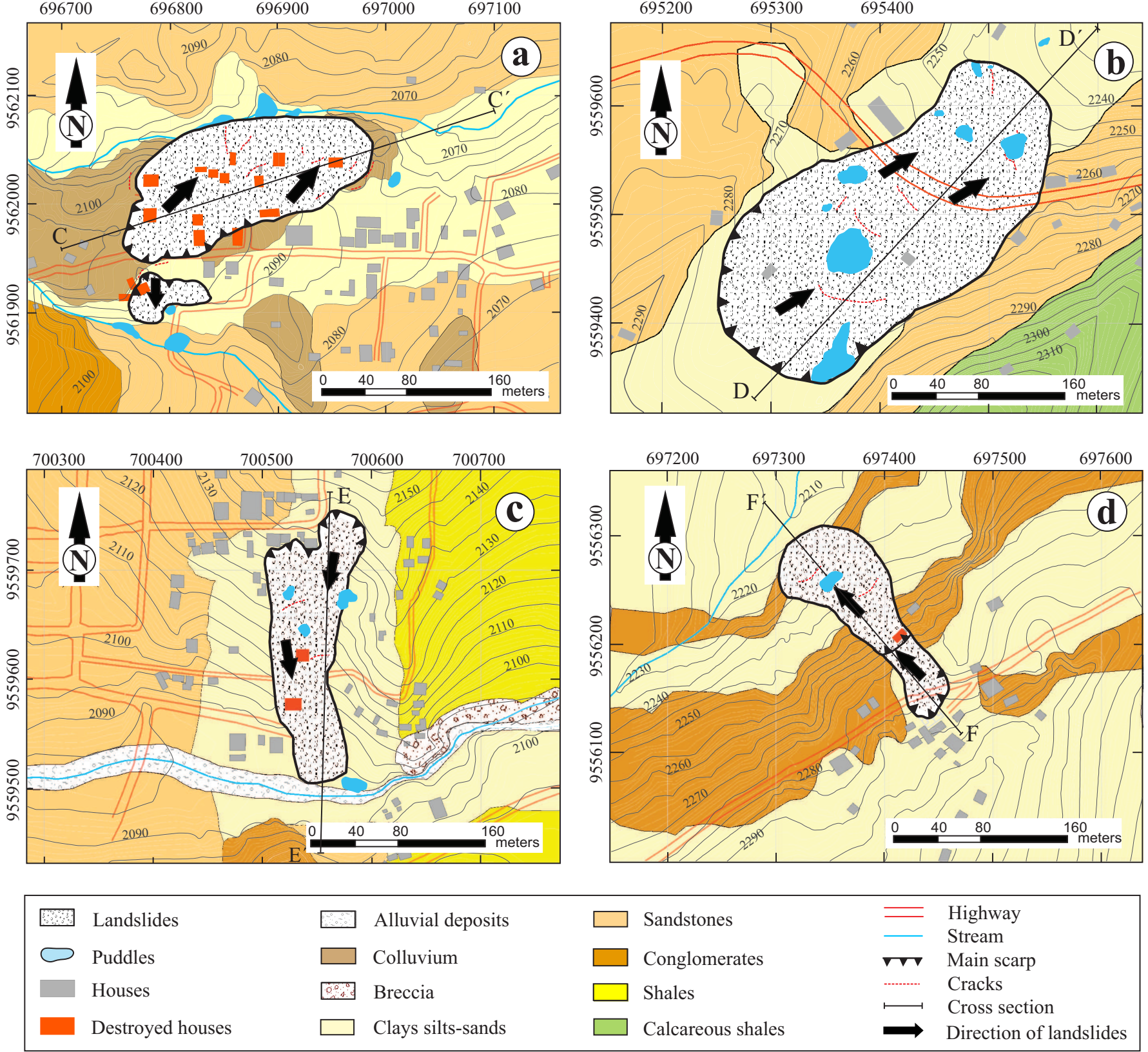
a
b
c
d
N
C
C´
D
D´
E
E´
F
F´
0 40 80 160 meters
Landslides
Puddles
Houses
Destroyed houses
Alluvial deposits
Colluvium
Breccia
Clays silts-sands
Sandstones
Conglomerates
Shales
Calcareous shales
Highway
Stream
Main scarp
Cracks
Cross section
Direction of landslides

Figure 10

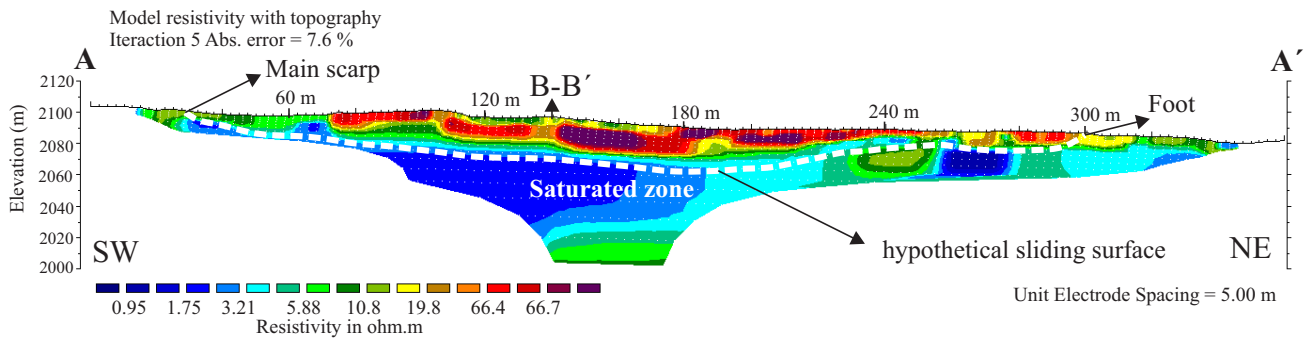
a
Model resistivity with topography
Iteraction 5 Abs. error = 7.6 %
A
A´
Main scarp
60 m
120 m
B-B´
180 m
240 m
300 m
Foot
Elevation (m)
2120
2100
2080
2060
2040
2020
2000
Saturated zone
SW
hypothetical sliding surface
NE
0.95 1.75 3.21 5.88 10.8 19.8 66.4 66.7
Resistivity in ohm.m
Unit Electrode Spacing = 5.00 m

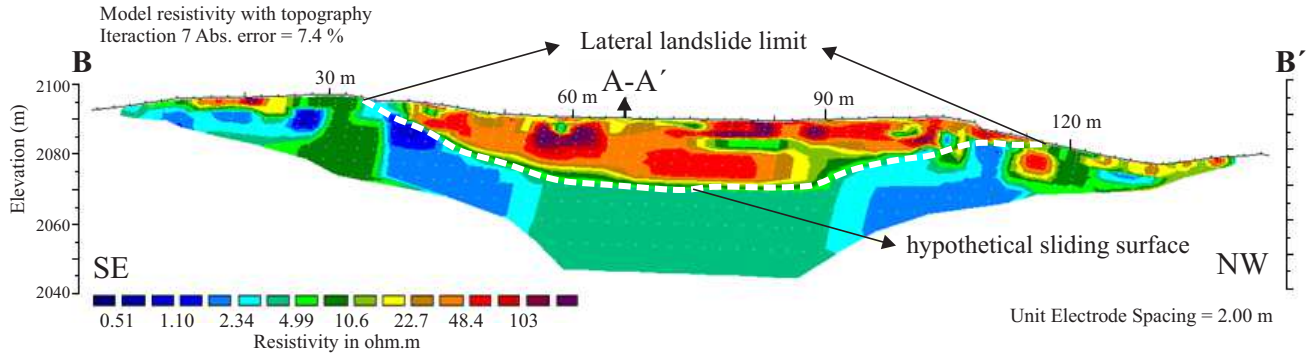
Model resistivity with topography
Iteraction 7 Abs. error = 7.4 %
B
B´
Lateral landslide limit
30 m
A-A´
60 m
90 m
120 m
Elevation (m)
2100
2080
2060
2040
SE
hypothetical sliding surface
NW
0.51 1.10 2.34 4.99 10.6 22.7 48.4 103
Resistivity in ohm.m
Unit Electrode Spacing = 2.00 m

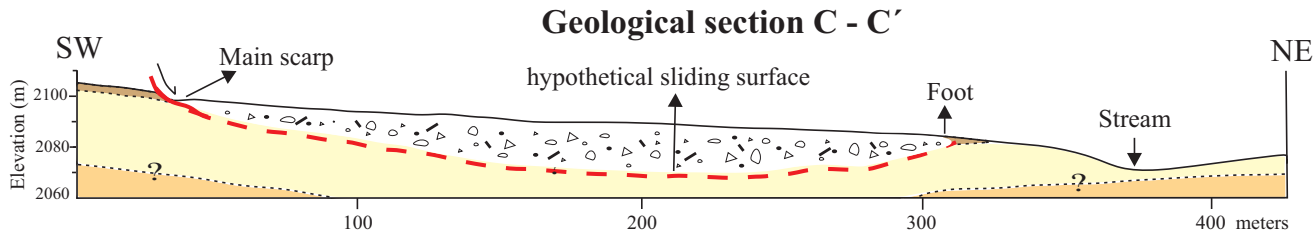
Geological section C - C´
SW
NE
Main scarp
hypothetical sliding surface
Foot
Stream
Elevation (m)
2100
2080
2060
?
100
200
300
400 meters

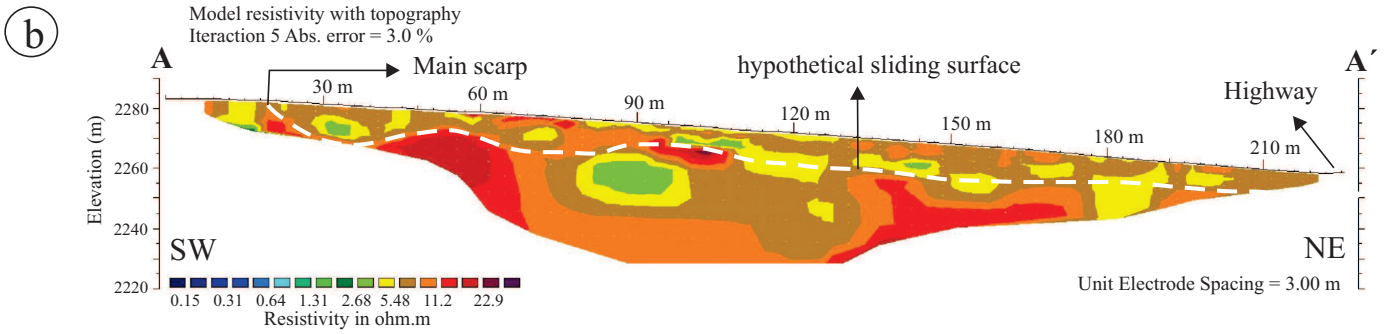
b
Model resistivity with topography
Iteraction 5 Abs. error = 3.0 %
A
A´
Main scarp
hypothetical sliding surface
30 m
60 m
90 m
120 m
150 m
180 m
210 m
Highway
Elevation (m)
2280
2260
2240
2220
SW
NE
0.15 0.31 0.64 1.31 2.68 5.48 11.2 22.9
Resistivity in ohm.m
Unit Electrode Spacing = 3.00 m

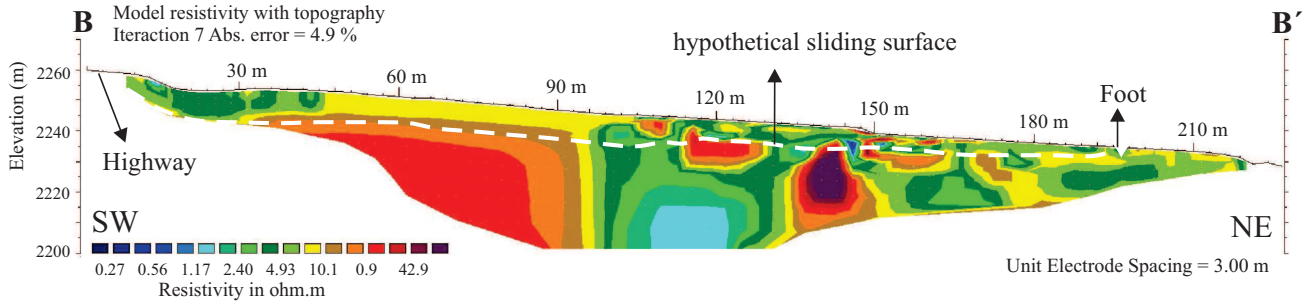
B
Model resistivity with topography
Iteraction 7 Abs. error = 4.9 %
B´
hypothetical sliding surface
30 m
60 m
90 m
120 m
150 m
180 m
Foot
210 m
Highway
Elevation (m)
2260
2240
2220
2200
SW
NE
0.27 0.56 1.17 2.40 4.93 10.1 0.9 42.9
Resistivity in ohm.m
Unit Electrode Spacing = 3.00 m

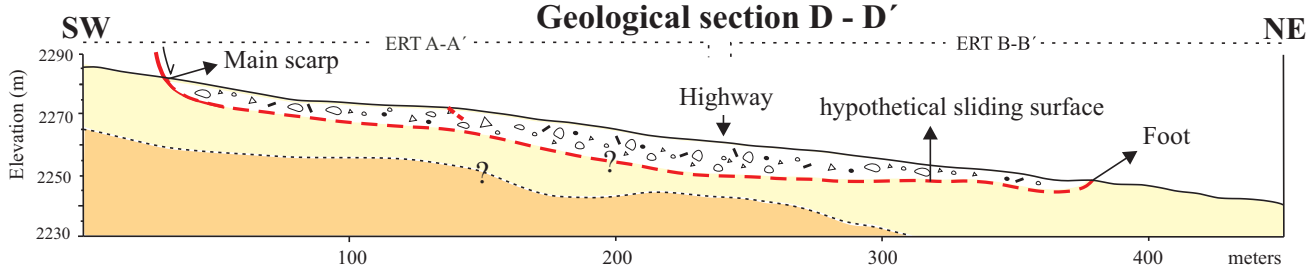
Geological section D - D´
SW
ERT A-A´
ERT B-B´
NE
Main scarp
Highway
hypothetical sliding surface
Foot
Elevation (m)
2290
2270
2250
2230
?
100
200
300
400
meters


Landslides
Colluvium
Clays silts-sands
Sandstones

Figure 11

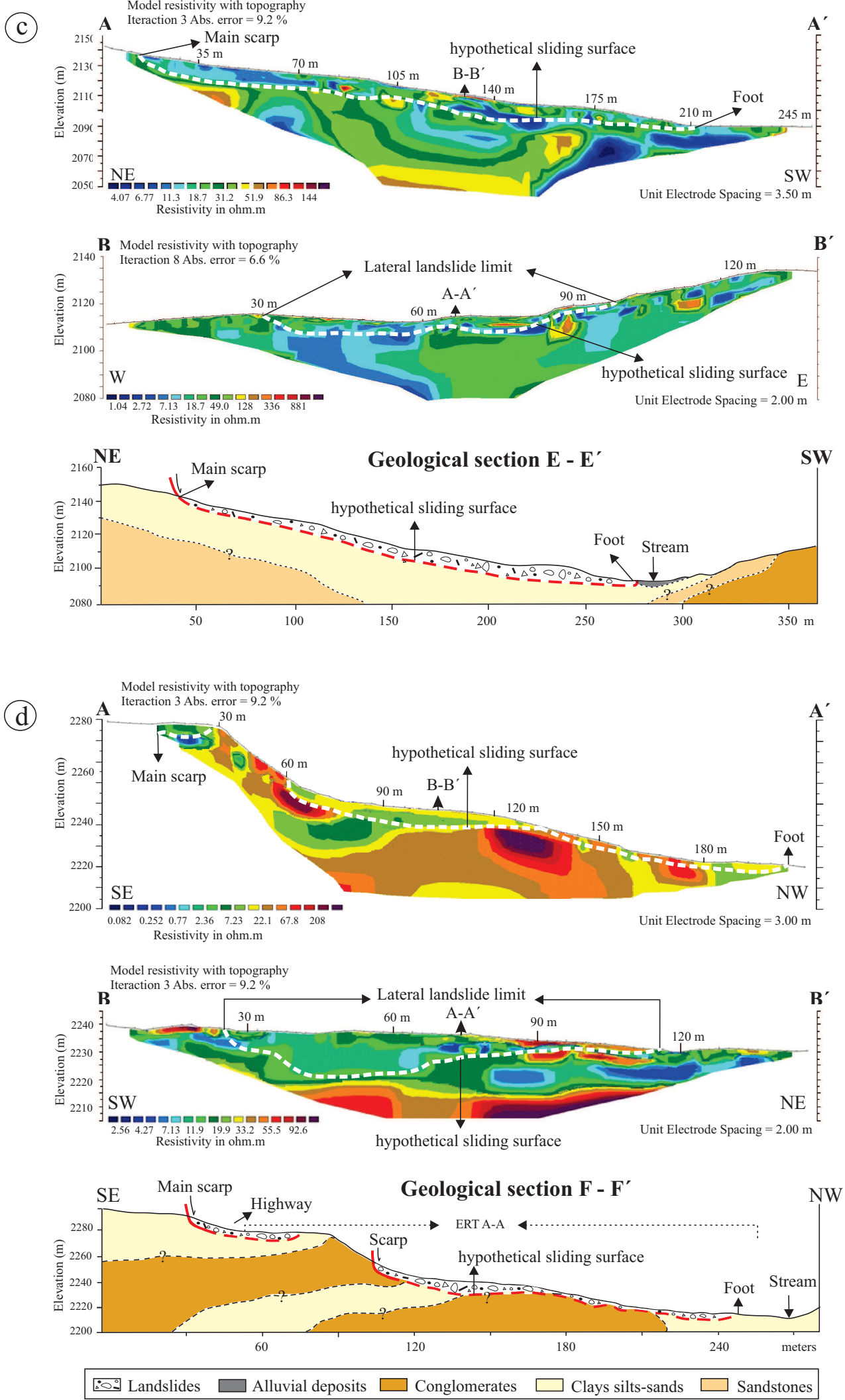
c
Model resistivity with topography
Iteraction 3 Abs. error = 9.2 %
A
A´
Main scarp
35 m
70 m
105 m
B-B´
140 m
175 m
210 m
Foot
245 m
hypothetical sliding surface
Elevation (m)
NE
SW
4.07 6.77 11.3 18.7 31.2 51.9 86.3 144
Resistivity in ohm.m
Unit Electrode Spacing = 3.50 m
B
B´
Model resistivity with topography
Iteraction 8 Abs. error = 6.6 %
Lateral landslide limit
30 m
60 m
A-A´
90 m
120 m
hypothetical sliding surface
W
E
1.04 2.72 7.13 18.7 49.0 128 336 881
Resistivity in ohm.m
Unit Electrode Spacing = 2.00 m
Geological section E - E´
NE
SW
Main scarp
hypothetical sliding surface
Foot
Stream
Elevation (m)
50 100 150 200 250 300 350 m
d
Model resistivity with topography
Iteraction 3 Abs. error = 9.2 %
A
A´
30 m
60 m
90 m
B-B´
120 m
150 m
180 m
Foot
Main scarp
hypothetical sliding surface
SE
NW
0.082 0.252 0.77 2.36 7.23 22.1 67.8 208
Resistivity in ohm.m
Unit Electrode Spacing = 3.00 m
Model resistivity with topography
Iteraction 3 Abs. error = 9.2 %
B
B´
Lateral landslide limit
30 m
60 m
A-A´
90 m
120 m
SW
NE
2.56 4.27 7.13 11.9 19.9 33.2 55.5 92.6
Resistivity in ohm.m
hypothetical sliding surface
Unit Electrode Spacing = 2.00 m
Geological section F - F´
SE
NW
Main scarp
Highway
ERT A-A
Scarp
hypothetical sliding surface
Foot
Stream
Elevation (m)
60 120 180 240 meters
Landslides
Alluvial deposits
Conglomerates
Clays silts-sands
Sandstones

Figure 12

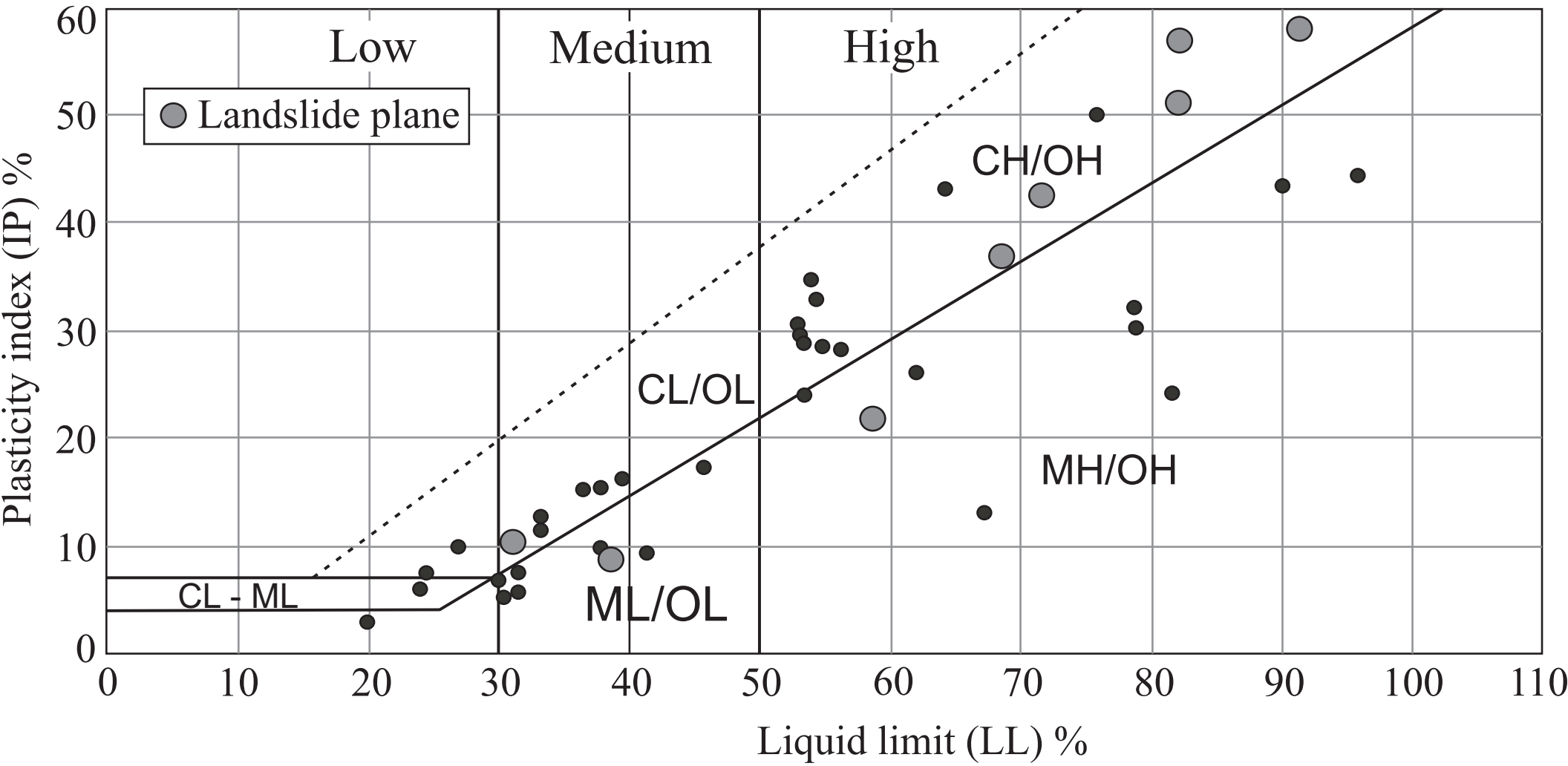
Low
Medium
High
Landslide plane
CH/OH
CL/OL
MH/OH
CL - ML
ML/OL
Plasticity index (IP) %
Liquid limit (LL) %
0
10
20
30
40
50
60
70
80
90
100
110